Laboratori Nazionali di Frascati

LNF-89/074(P)
2 Novembre 1989

A. Marcelli:

HIGH RESOLUTION POLARIZED X RAY ABSORPTION SPECTROSCOPY: SYMMETRY OF THE HOLE STATES IN THE HIGH T_C SUPERCONDUCTORS

To be published on
"Studied of High Temperature Superconductors "
Ed. by A.V. Narlikar - Nova Science Publisher -ISBN Vol. 4 (1989)

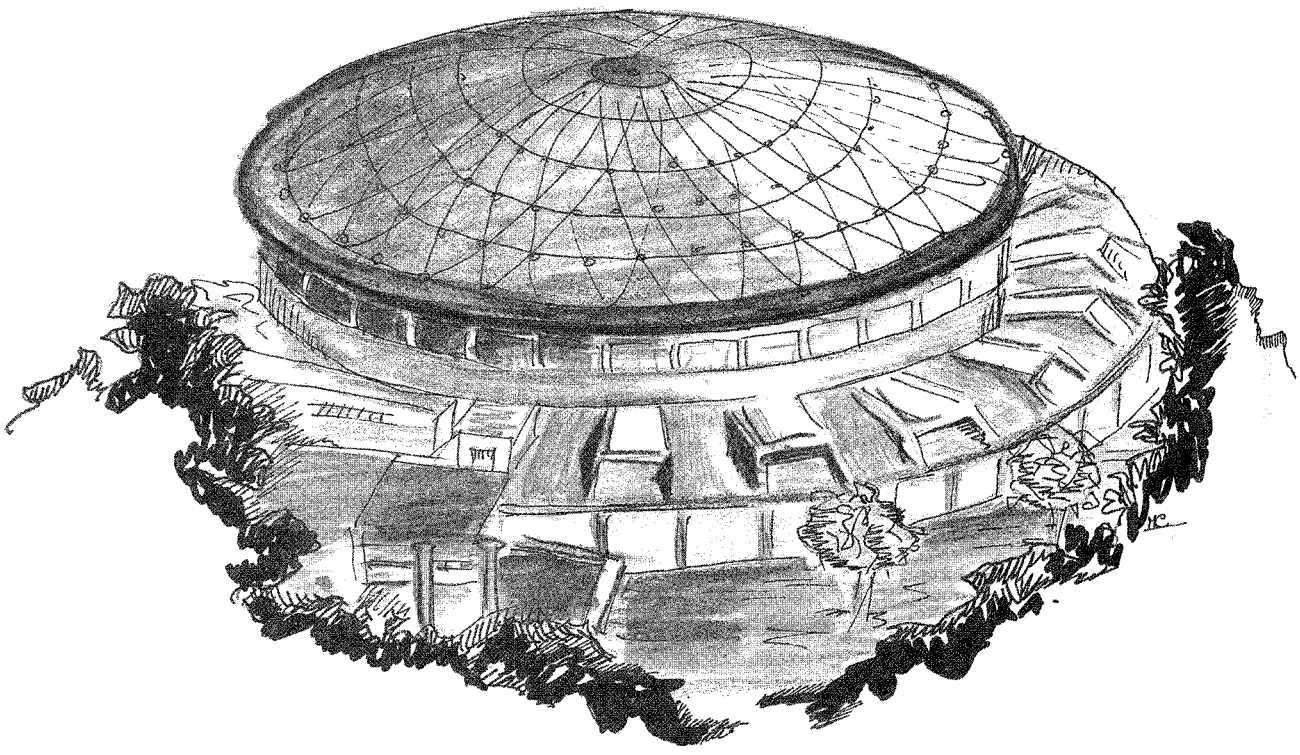

Servizio Documentazione
dei Laboratori Nazionali di Frascati
P.O. Box, 13 - 00044 Frascati (Italy)

INFN - Laboratori Nazionali di Frascati
Servizio Documentazione

LNF-89/074(P)
3 Novembre 1989

HIGH RESOLUTION POLARIZED X RAY ABSORPTION SPECTROSCOPY: SYMMETRY OF THE HOLE STATES IN THE HIGH T_C SUPERCONDUCTORS

A. Marcelli
INFN - Laboratori Nazionali di Frascati, P.O. Box 13, 00044 Frascati, Italy

INTRODUCTION

Oxygen deficient-perovskite materials with expected non integer formal valence state of the Cu ions higher than two, have first attracted the scientific interest of the group of Caen university [1-3] because some of these ceramic materials are very good conductors at room temperature. Following the discovery of the high temperature superconductivity in this class of materials [4,5] an impressive number of scientific investigation have been carried out on the electronic structure of these systems to understand the microscopic mechanism of high temperature superconductivity.

Principal aim of this short review is to underline, in the dark jungle of the experimental techniques, the role of the x-ray absorption spectroscopy (XAS) as one powerful technique to investigate high temperature superconductors materials. Recent results obtained by polarized x-ray absorption spectroscopy with synchrotron radiation and polarized x-ray absorption calculation in the frame of the multiple scattering theory on high temperature superconductors are reported. They show that XAS can be used to investigate not only the amounts of Cu^{1+}, Cu^{2+} or Cu^{3+} configurations in the ground state and their relative changes with the oxygen content, moreover the detection of the symmetry of the hole state can be obtained giving unique information on the electronic states near the Fermi energy.

Core level spectroscopies provide a direct tool to investigate the electronic structure and the charge carriers in these materials. [6] In particular x-ray photoemission spectroscopy (XPS) [7-12] is essentially determined by the initial density of occupied states.
Resonant XPS experiments at the Cu 3p threshold which shown the presence of strong electron correlation around the copper atoms demonstrate the existence of a two-hole bound state, [10,13-17] while Cu 2p XPS shown the close similarity between high temperature superconductors and charge transfer type insulators [18] and strongly suggest superconductivity mechanism via oxygen 2p holes. [7,19-21]

Core-level x-ray absorption spectroscopy (i.e. at copper K-edge, [22-27] at copper L_3-edge, [28-31] and at oxygen K-edge [20]) probes the different unoccupied electronic states of angular moment $\ell' = \ell \pm 1$ at selected atomic sites, moreover polarized x-ray absorption spectroscopy spectra probe the orientation of the unoccupied orbitals. Thus polarized XAS spectroscopy of a single crystal is a suitable probe to determine experimentally the symmetry of the molecular orbitals where the electronic holes induced by doping in a deficient-perovskite are formed.

In the classical quantum theory the absorption cross section is given by many-body excitations of the N-electron system. Following the interaction with the photon beam with energy ω, the system is excited from the initial state i at energy E_i to a final state f at energy E_f. In the one-electron approximation the x-ray absorption is described by single-particle processes. The N-electron system is separated into two parts: the single electron in the core level which is excited into an unoccupied level and the N-1 passive electrons which do not participate directly in the electronic transition. The one-electron transition takes place in a static potential determined by a single configuration of the N-1 passive electrons.

The absorption coefficient $\mu_C(E)$ for the transitions from the core level $c(n,\ell,J)$ with energy E_c and wavefunction φ_{cM}, in the one-electron approximation, can be expressed in atomic units as

$$\mu_C(E) = 4\pi^2 \alpha F_C(E)/(\Omega/\nu) \qquad E>E_F \tag{1}$$

where $\alpha^{-1}=137.036$ is the inverse fine-structure constant, Ω is the volume of the primitive cell, ν is the number of contributing atoms in the primitive cell and $F_C(E)$ is the spectral distribution of oscillator strength [32]

$$F_C(E)= (\omega/3) \sum_{\mathbf{k},j} \sum_{M=-J} r^2_{cM,\mathbf{k}j} \delta(E - E_{\mathbf{k}j}) \tag{2}$$

$$r_{cM,\mathbf{k}j} = \int \varphi_{cM}(r)\, r\, \Psi_{\mathbf{k}j}(r)\, d^3r = \langle \varphi_{cM} \mid r \mid \Psi_{\mathbf{k}j} \rangle \tag{3}$$

$\Psi_{\mathbf{k}j}$ and $E_{\mathbf{k}j}$ are the wavefunction and energy of the j-th conduction band at reduced vector $\mathbf{k}$, ω is the photon energy $\omega = E - E_c$ and the integration is carried out over the volume of the primitive cell. Since the dipole transitions dominate the process of photoabsorption, an electron from a core level having angular momentum ℓ is excited into the $\ell \pm 1$ final states. Neglecting the spin-orbit coupling for the band states, $F_C(E)$ can be written as [33,34]

$$F_C(E) = (\omega/3)\, (2J+1)/2(2\ell+1)\, \{ \ell/(2\ell-1) f_{c,\ell-1}(E) + (\ell+1)/(2\ell+1)\, f_{c,\ell+1}(E) \} \tag{4}$$

where the partial strength $f_{c,\ell}(E)$ can be factorized into

$$f_{c,\ell}(E) = \rho_{c,\ell}\ N_\ell(E) \tag{5}$$

$N_\ell(E)$ is the angular projected density of states defined as

$$N_\ell(E) = 2 \sum_{\mathbf{k},j} \sum_m |\langle Y_{\ell m} \mid \Psi_{\mathbf{k}j} \rangle|^2\, \delta(E - E_{\mathbf{k}j}) \tag{6}$$

where the energy band states are labelled by the reduced wave vector $\mathbf{k}$ and the band index j. The effective matrix element $\rho_{c,\ell}(E)$ is given by

$$\rho_{c,\ell}(E) = \langle \varphi_c \mid r \mid \phi_\ell(E) \rangle^2 / \langle \phi_\ell^2(E) \rangle \tag{7}$$

where the wave function $\phi_\ell(E,r)$ is a solution of the radial Schrödinger equation inside the muffin-tin (MT) sphere of radius S ($r<S$), and outside the MT sphere ($r \geq S$), is given by

$$\phi_\ell(E,r) = [\cos \delta_\ell(E)]\, J_\ell[(E-V_O)^{1/2} r] - [\sin \delta_\ell(E)]\, n_\ell[(E-V_O)^{1/2} r] \tag{8}$$

where δ_ℓ (E) is the ℓ-th phase shift of the muffin tin potential, V_o is the muffin tin zero of the potential and J_ℓ and n_ℓ are spherical Bessel functions.

The spectra of crystals are therefore interpreted in terms of the product of the partial (of selected orbital momentum $\ell\pm1$) density of states and of the matrix element. Müller *et al.* [33,34] have shown that the x-ray absorption near edge structure (XANES) spectra can be understood as the product of an atomic-like term and a solid state term. The factorization of the partial oscillator strength into the solid state term χ_ℓ (E) and atomic term $f^{at}{}_{c,\ell}$ (E) is given by

$$f_{c,\ell}(E) = f^{at}{}_{c,\ell}(E) \cdot \chi_\ell(E). \tag{9}$$

The atomic term is obtained by considering a single muffin tin potential confined in the Wigner-Seitz (WS) sphere of radius S_{WS} and the spectrum for the transition from the core level in the single atom is

$$f^{at}{}_{c,\ell}(E) = (2\ell+1)\, N^{FE}(E) < \varphi_c \mid r \mid \phi_\ell(E,r) >^2 \tag{10}$$

where the integration is over the Wigner-Seitz (WS) sphere and $N^{FE}(E) = (E - V_o)^2/2\pi$ is the free electron density of states. The solid state term is

$$\chi_\ell(E) = N_\ell(E) / N^{at}{}_{c,\ell}(E) \tag{11}$$

where

$$N^{at}{}_{c,\ell}(E) = 1/\Omega\, (2\ell+1) N^{FE}(E) < \phi_\ell{}^2(E,r) > \tag{12}$$

is the projected density of states for the single-sphere problem.

This approach leads to the following understanding of the x-ray absorption spectra: i) the overall magnitude and shape of a particular spectrum is determined by the corresponding atomic transition rate $f^{at}{}_{c,\ell}(E)$ and ii) the fine structure of the spectrum is determined by the solid state factor χ_ℓ (E) which is proportional to the density of band states with $\ell\pm1$ orbital characters. The ℓ-1 term is often ignored because usually it exhibits a much smaller amplitude than the ℓ+1 term. However in some cases, like in the first six electron volt above threshold in the Si L_3-edge, the ℓ+1 density of states is negligible and the ℓ-1 term is the most important.

In some cases the atomic part exhibits strong resonances in a small energy range therefore the contribution of the solid state factor $\chi_\ell(E)$ can be neglected. In these cases the spectra of solids can be interpreted in terms of atomic transitions (see for examples the $L_{2,3}$ edges of Ni and Cu in insulating systems). [35-37] In other cases the atomic part exhibits a smooth structureless spectrum over a large energy range and therefore the spectral features can be assigned to the solid state factor χ_ℓ (E).

In the case of metals, the core hole in the static final state potential is fully screened by valence electrons close to the Fermi level. Most of the XANES spectra, in this case, can be interpreted in the frame of the von Barth and Grossmann final state rule, [38,39] which states that the wave function of the excited photoelectron is determined by the final state potential with the core hole and the relaxed N-1 electrons. Therefore in most cases the one-electron transitions are assumed to take place in the potential of the fully relaxed configuration of the N-1 passive electrons in the presence of the core hole. The fully relaxed configuration is defined as the final state many-body configuration with the lowest energy. The final state rule breaks down for transitions to nearly filled bands like in the case of $2p \rightarrow$ ed transition in palladium or in nickel metal.

Many-body effects in XANES can arise because of the presence of different many-body final state configurations of the N-1 passive electrons. Configuration interaction of many-body

interaction in the ground state like in valence fluctuating materials [40] or correlated systems such as NiO, CeO_2, PrO_2 and CuO. The electronic structure of these insulating correlated oxides has been object of large interest in these last years. [41,42] In these compounds a strong hybridization between a localized metal orbital and the delocalized 2p oxygen states coexist with a large electronic d-d or f-f Hubbard repulsion. The cuprate high-T_C superconductors belong to this class of materials. The specific electronic structure of these systems is characterized by localized states on the metal sites with a large electronic correlation. The ground state of the system can be described by mixing of localized Cu $3d^9$ and Cu $3d^{10}\underline{L}$ configurations where $\underline{L}$ indicates a hole in the oxygen derived valence band. In the stoichiometric insulating systems the two ionic configurations are separated by the energy ΔE. The mixing between the localized electronic configurations is due to a large oxygen-metal hybridization T ($T \sim \Delta E$).
This type of electronic structure is possible, when some orbitals have an atomic-like localized character, the energy separation between the delocalized ligand band and the localized metal orbital is negligible and there is a large metal oxygen covalency. This seems to be the case of high temperature superconducting perovskites where the Cu 3d states are atomic-like and both the metal 3d and the oxygen 2p band cross the Fermi level. [6] Moreover since the first experimental investigation by core-level spectroscopies [7,8,28,29] the d-d Coulomb repulsion and the Cu-O hybridization energies were found to be about 6-8 eV and 2-3 eV respectively.

POLARIZED X-RAY ABSORPTION SPECTROSCOPY

Polarized x-ray absorption spectra show a strong dichroism for anisotropic sites. The strong dichroism of XANES spectra of single crystals was observed by several groups and in different materials. [43-57] The dichroism for electronic transitions is well known in the classical quantum theory of the absorption cross section. By the interaction with the photon beam the system is excited from the initial state i at energy E_i to the final state f at energy E_f and in the dipole approximation the total absorption cross section is given by

$$\sigma(\omega) \sim \omega \sum_f |M_{if}|^2 \delta(E_i - E_f + \omega) \tag{13}$$

where the sum is extended over all the possible final states f and M_{if} is the matrix element involving the initial Ψ_i and final Ψ_f^* many-body radial wave functions

$$M_{if} = \int \Psi_f^*(r_1, r_2, \ldots, r_n) \sum_n (\mathbf{r}_n \cdot \mathbf{E}) \Psi_i(r_1, r_2, \ldots, r_n)\, dr \tag{14}$$

where $\mathbf{E}$ is the unitary polarization vector of the electric field and the $\mathbf{r}_n$ is the vector describing the position of the n-th electron. Therefore, in anisotropic systems the matrix element is dependent on the direction of the polarization vector via the terms $(\mathbf{r}_n \cdot \mathbf{E})$.
In the multiple scattering description of the absorption cross section in real space the polarization effects are determined by combination of terms like $|(\mathbf{r}_i \cdot \mathbf{E})|^2$ where $\mathbf{r}_i$ are the positions of neighboring atoms respect with the central absorbing atom. Just one term of this type remains in the single scattering approximation which describe the polarized extended x-ray absorption spectra (EXAFS) [54] in which oscillations originating at a particular scattered atom can appear or disappear depending on whether the electric field is directed towards that atom or not. This property has been widely used in surface EXAFS studies to determine separately the interatomic distances parallel and normal to the surface plane. [55,56]

The multiple scattering contributions due to a set of atoms in a particular direction or on a plane can be selected in the XANES spectra of anisotropic clusters using the polarization dependence of the absorption cross section Therefore, the orientation and angular distribution of neighboring atoms can be determined by changing the relative position of the incident beam.

Fig. 1 reports the vanadium K-edge XANES spectra of a spontaneously dehydrated sol-gel sample of V_2O_5. This sample is formed of oriented sheets separated by about 10 Å of water molecules. Each sheet consists of square plane bipyramid with the base on the xy plane and a

on the other side, in the z direction. The experimental spectra for the electric field E oriented along the z direction (E||z) and parallel to sheet planes (E⊥z) are shown. These spectra are a good example of angular resolved XANES because the dichroism is very large and it appears both in the threshold region for the molecular like bound excitations, giving the white line, and in the continuum region. The white line is completely suppressed for the polarization vector oriented on the plane, showing that it is produced by the short double V-O bond. [52]

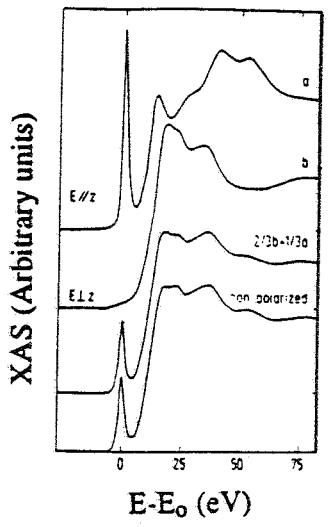

FIG. 1 - Polarized experimental XANES spectra of V_2O_5 dehydrated sol-gel. Curve a: the electric field E is parallel to the normal z of the V_2O_5 layers, i.e. along the axis of the square pyramids; curve b: the electric field E is parallel to the V_2O_5 layers; the lowest curve is the unpolarized spectrum and above it the the weighted spectrum from the two polarized spectra.

The interpretation of polarized XANES spectra in terms of multiple scattering allows the determination of the role of a selected group of atoms. This is illustrated in Fig. 2 where the angular resolved XANES calculations are reported for two type of VO_6 clusters. The calculation clearly shows that the white line appears only with the electric field along the V-O double bond. The main features of the experimental spectrum (E||z) are well reproduced by theoretical calculations for both clusters with and without (upper curve) vanadium atom on the xy plane.

The interpretation of angular resolved XANES is very useful for understanding and interpreting the spectra of unpolarized spectra. Some features in unpolarized spectra can be assigned to multiple scattering with a selected number of atoms, like for the structures at about 25 eV and that at 60 eV in the unpolarized spectrum in Fig. 1 which can be associated with multiple scattering in the plane and along the normal respectively. Starting with simple models a qualitative agreement with experimental results can be reached which is improved as soon as more complicated clusters are used.

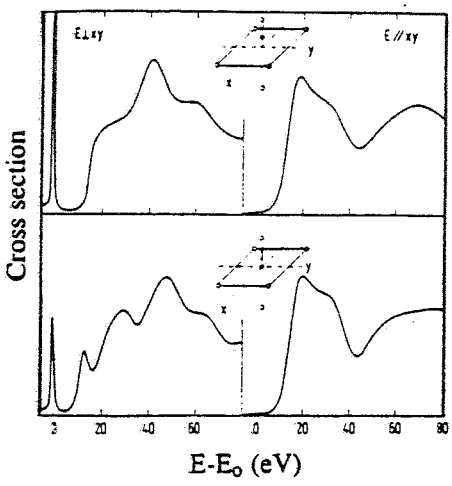

FIG. 2 - The theoretical angular resolved multiple scattering calculation for a square bipyramid with a short double V-O bond (d=1.58Å) and with a long V-O bond (d=2.6Å) along the z axis due to the oxygen of a water molecule and four oxygens on the xy plane at 2.0 Å. Polarized spectra with the V out of plane by 0.5 Å (upper curves) and for a similar cluster with the same distances but the with the V atom in the plane (lower curves).

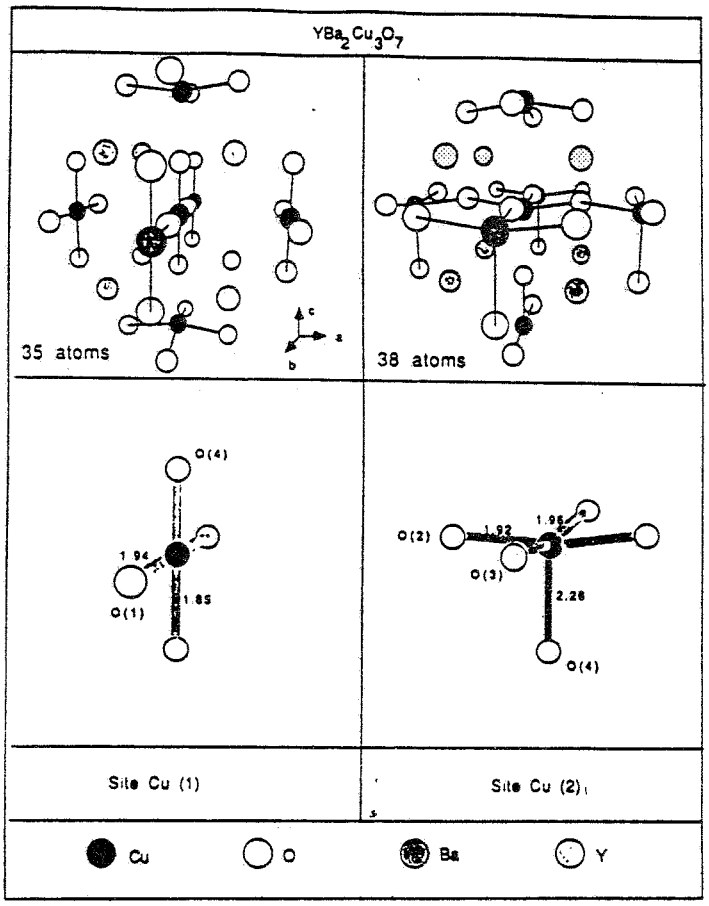

FIG. 3 - Structure of the clusters of neighbor atoms surrounding the Cu(1) and Cu(2) sites in $YBa_2Cu_3O_7$.

The Angular Resolved XANES at the Cu K-edge

Due to the local character of this experimental probe, angular resolved XANES are used to determine the orientation of biological complexes and of chemisorbed molecules on surfaces. [49,57,58] Recently was applied to the study of the Cu K-edge XANES to determine the structural changes associate with the loss of oxygen going from the high temperature superconductor $YBa_2Cu_3O_7$ to the antiferromagnetic insulator $YBa_2Cu_3O_6$. [26,27,59-63]

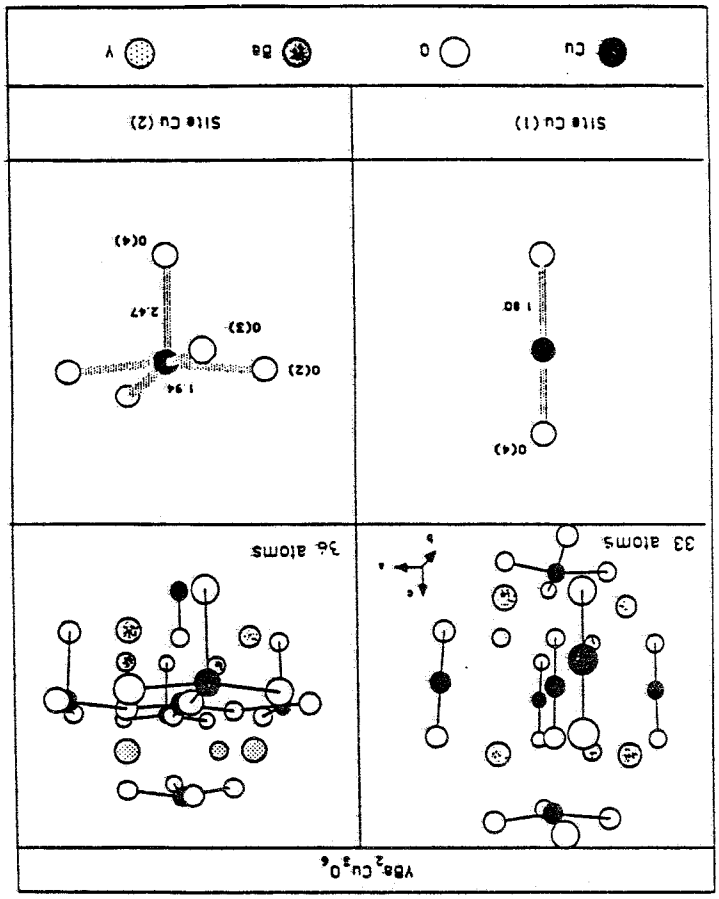

FIG. 4. - Structure of the clusters of neighbor atoms surroundings the Cu(1) and Cu(2) sites in $YBa_2Cu_3O_6$.

XANES calculation in the frame of multiple scattering (MS) theory has been performed to interpret a large variety of materials, from the transition metal oxides, to biological molecules andmolecular complexes and recently to the study of the distortions of Cu site. [64]

In the case of copper oxides the orthorhombic crystalline structure of $YBa_2Cu_3O_7$ changes to the tetragonal structure of $YBa_2Cu_3O_6$ (see for example Cava, *et al.*, [65]). There are two types of Cu sites, named Cu(1) and Cu(2), in the crystalline cell. Therefore two clusters of about 35 atoms, relevant for the Cu K-edge XANES, within a sphere of 5Å radius around each of the two central Cu ions for $YBa_2Cu_3O_7$ ($YBa_2Cu_3O_6$), are shown in Fig.3 (Fig.4). [66]

The Cu K-edge XANES probes the local structure of a cluster of atoms of finite size

multiple scattering approach, to get an an agreement with the experimental data a large clusters of about 35 atoms within a sphere of 5Å radius was necessary. [67] In agreement with the experimental data on the copper K-edge, multiple scattering calculation shows that changes in the XANES spectra induced by oxygen vacancies are the elongation of the Cu(2)-O(4) distance (between the Cu(2) in the CuO_2 plane and its apical oxygen) which induces the shift of the main peak in the polarized XANES spectra with **E**||**c** toward lower energy. The formation of the oxygen vacancies induces changes also in the **E**⊥**c** spectra for the Cu(1) ion in the linear chains. [66]

Starting from the oxygen rich phase $YBa_2Cu_3O_7$ the structural changes observed in the Cu coordination spheres by multiple scattering calculation are:
i) the Cu ion in site Cu(1) changes from a square plane configuration with 4 oxygens in the **bc** plane (Fig. 3) to a linear coordination (Fig. 4) in $YBa_2Cu_3O_6$;
ii) the Cu ion in site Cu(2) has a fivefold square pyramid configuration where the Cu(2)-apical oxygen O(4) distance changes from 2.26 Å to 2.47 Å in $YBa_2Cu_3O_6$.
The axial distances of Cu(1)-O(4) and Cu(2)-O(4), measured by neutron diffraction experiments [65], are shown in Table I. Moreover the different Cu(2)-O(2) and Cu(2)-O(3) nearest neighbor distances (Fig. 3) become the same in tetragonal $YBa_2Cu_3O_6$ (Fig. 4).

TABLE I

Axial distances from neutron diffraction data [65]

oxygen stoichiometry 7-x	0.0	0.2	0.5	1.0
Cu(1)-O(4) distance (Å)	1.84	1.84	1.79	1.79
Cu(2)-O(4) distance (Å)	2.30	2.32	2.43	2.47

The **E**⊥**c** polarized Cu K-edge XANES of single crystals of $YBa_2Cu_3O_{7-x}$ has been measured for two different oxygen concentration (x=0.15 and x=0.8) by Tolentino *et al.* [62] The main difference between the two spectra is the presence of two peaks at 1.6 and 8.6 eV (the zero in energy has been chosen at the first point of inflection of the absorption spectrum of metallic Cu, E_0=8976 eV). These peaks are associated to the formation of linear chains Cu(1)O(4) along the **c** axis, and to the change of formal valence of the Cu(1) from +2 to +1 (i.e. from the electronic configuration mainly $|3d^9\underline{L}\rangle$ to mainly $|3d^{10}\rangle$). Moreover only a red-shift in energy of about 1 eV has been found in unpolarized XANES [62] going from x=0.05 to x= 0.15 in agreement with findings of several groups. [59,61,63,68].
This calculation shows that changes of the XANES spectra going from $YBa_2Cu_3O_7$ to $YBa_2Cu_3O_6$ are due to structural changes in the Cu coordination shells based on changes in the local structure induced by depletion of oxygen.

The E||c polarized XANES spectra. The main changes observed [68] in the polarized E||c XANES spectrum going from $YBa_2Cu_3O_7$ to $YBa_2Cu_3O_6$ are: i) a red-shift of the energy of the absorption edge (features at 7.3 eV and at 14.6 eV) and ii) a lowering of the intensity of the main absorption peak (at 17.1 eV), both measured relative to the Cu metal K-edge for $YBa_2Cu_3O_7$.
The crystallographic data show that in the direction of the **c** axis, the main structural changes are: i) the contraction of the axial distance Cu(1)-O(4) and ii) the elongation of Cu(2)-O(4) distance, as shown in Fig. 3.

It is well established that the bond length variations induce an energy shift of the XANES peaks according with the rule $(E_\sim - E_\sim)d^2$ = constant (in which $E_\sim$ is a reference energy and d is

$\Delta d/d$. In order to test this rule, XANES have been calculated using as reference energy the intersphere constant V_O, which is the value of the potential in the interstitial volume between the muffin tin spheres, for both linear and square plane coordinated copper ions by varying the Cu-O distance in the range 1.85<d<3.5 Å. Fig. 5. shows that these calculations give an important deviation from the linear trend for d >2.6 Å. Therefore a linear red-shift versus decreasing $1/d^2$ (increasing bond distance) in the range of Cu-O distances 1.8<d<2.5 Å is expected.

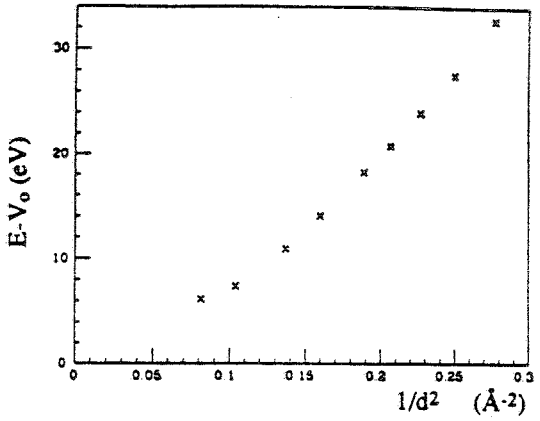

FIG. 5. - Energy of the strongest peak in Cu K edge XANES due to the multiple scattering resonance determined by the first shell of oxygens for a CuO_2 linear cluster as a function of $1/d^2$ where d is the Cu-O distance.

The calculated **E**||**c** XANES for the two $Cu(1)O(4)_2O(1)_2$ and $Cu(2)O(2)_2O(3)_2O(4)$ clusters for $YBa_2Cu_3O_7$ are compared in Fig. 6 with $Cu(1)O(4)_2$ and $Cu(2)O(2)_2O(3)_2O(4)$ for $YBa_2Cu_3O_6$. The variation observed in the spectrum of $Cu(2)O(2)_2O(3)_2O(4)$ going from $YBa_2Cu_3O_7$ to $YBa_2Cu_3O_6$ in panel b gives an energy red shift induced by the elongation of the Cu(2)O(4) distance by 0.21 Å.

The small contraction of the Cu(1)O(4) distance and the change of the overall shape of the **E**||**c** spectrum of Cu(1) site (panel a) due to the change from square plane to linear coordination, induces a blue shift.

The experimental polarized spectra are determined by the weighted sum 1:2 of the spectra of Cu(1) and Cu(2) site. The sum of the two spectra is shown in Fig. 6, panel c. The weighted sum of the two sites, is in good agreement with the experiment of Heald, *et al.*, [68] moreover the calculated spectra predict the lowering of intensity of the main absorption peak (about 9% from theory, versus 5% from experiment). The calculated energy interval between the shoulder on the rising edge and the main peak in calculation is about 12 eV, and it is consistent with experimental. The missing peak at 14.6 eV is assigned to a contribution of further shells.

The **E**⊥**c** polarized XANES spectra. The experimental data of Tolentino, *et al.*, [62] show the formation of two peaks named A and B at 1.6 and 8.6 eV respectively and the lowering of the main peak D at 16.5 eV going from $YBa_2Cu_3O_7$ to $YBa_2Cu_3O_6$. The main structural changes in the directions parallel to the **ab** plane are the missing of O(1) ions in the Cu(1) site of $YBa_2Cu_3O_6$. Looking at both Fig. 3 and 4 the Cu(2) clusters of the two crystalline structures are very similar up to the 3th shell, therefore in the **E**||**ab** polarized Cu XANES spectra the most prominent differences are expected to arise only from the site Cu(1).

Fig. 7 shows the results of the XANES calculation of the same clusters as in Fig. 6 but for the $\mathbf{E} \perp \mathbf{c}$ polarization. The spectra for the Cu(2) sites, on panel b, exhibits only small differences between the two compounds that can be assigned to the orthorhombic to tetragonal transition, and to the effect of changing Cu(2)O(4) distance. The XANES calculation for the Cu(1) cluster in panel a shows a large change determined by the fact that there are no atoms in the **ab** plane in the Cu(1) site of $YBa_2Cu_3O_6$, therefore the spectrum $\mathbf{E} \perp \mathbf{c}$ of Cu(1) in $YBa_2Cu_3O_6$ is determined mainly by the atomic muffin tin potential.
The spectrum c in the bottom of Fig. 7 is obtained summing the absorption of the two sites, and shows only the main absorption peak similar to experimental finding by Tolentino, *et al.*, [62] without the features A and B.

In Fig. 8 the calculation of the polarized $\mathbf{E} \perp \mathbf{c}$ XANES for the Cu(1) site for a larger cluster including the second shell of 8 Ba ions shows two new features A and B in the spectra of $YBa_2Cu_3O_6$, at energy ~ 1.5 and ~10 eV. The difference spectrum between the calculated spectra, shown in Fig. 6, reproduce well the experimental features named A, C and D in the difference spectrum of the experimental results [62] while a difference of about 1.5 eV for the B feature remains.

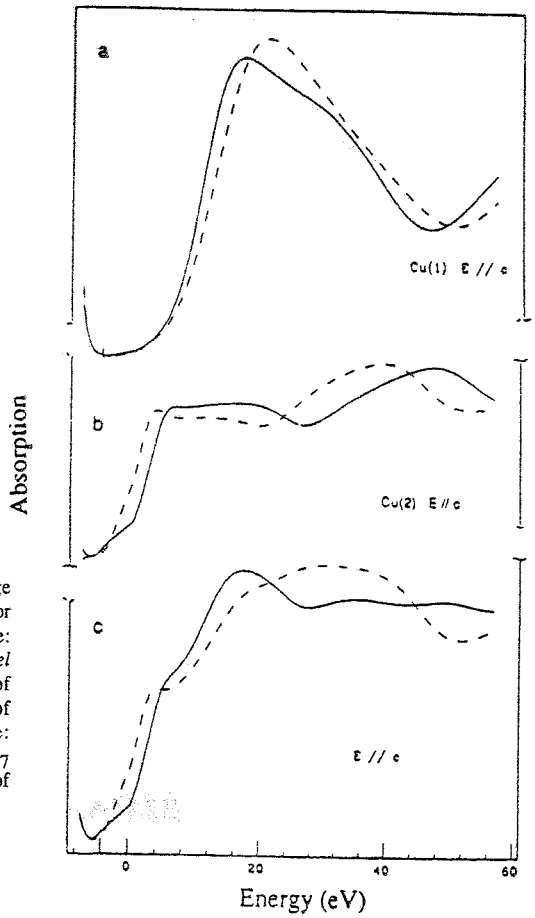

FIG. 6. - Calculated polarized Cu K-edge XANES with the electric field E||c axis for one oxygen shell clusters. Solid line: $YBa_2Cu_3O_7$, dashed line $YBa_2Cu_3O_6$. *Panel a)* Cu(1) site: $Cu(1)O(4)_2O(1)_2$ cluster of $YBa_2Cu_3O_7$ and $Cu(1)O(4)_2$ cluster of $YBa_2Cu_3O_6$, *panel b)* Cu(2) site: $Cu(2)O(2)_2O(3)_2O(4)$ cluster for $YBa_2Cu_3O_7$ and for $YBa_2Cu_3O_6$, *panel c)* weighted sum of the two Cu sites in the unit cell.

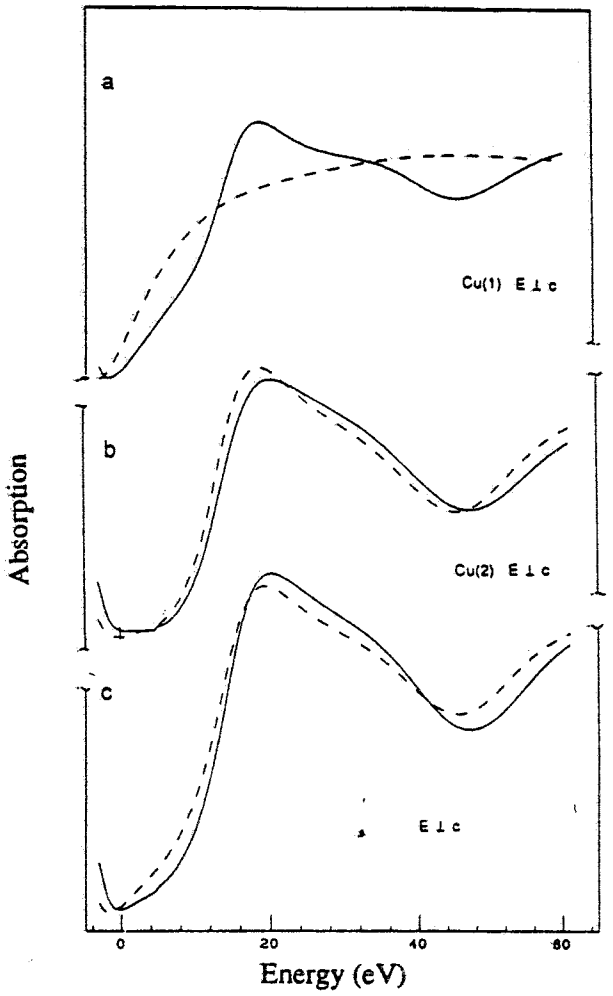

FIG. 7 - Calculated polarized Cu K-edge XANES with the electric field $\mathbf{E} \perp \mathbf{c}$ axis, for one oxygen shell cluster. Solid line $YBa_2Cu_3O_7$, dashed line $YBa_2Cu_3O_6$. From top to bottom as in Fig. 6, a) Cu(1) site, b) Cu(2) site, c) weighted sum of the two Cu sites in the unit cell.

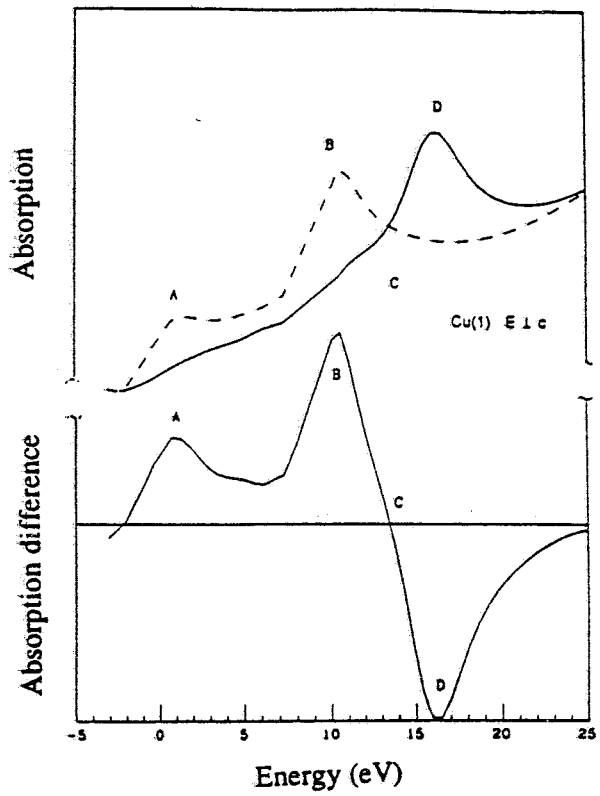

FIG. 8. - Upper panel: calculated polarized Cu K-edge XANES of Cu(1) site for two shell clusters (including Ba ions) with the electric field $\mathbf{E} \perp \mathbf{c}$ axis. Solid line $YBa_2Cu_3O_7$, dashed line $YBa_2Cu_3O_6$. Lower panel: difference between the spectra of $YBa_2Cu_3O_6$ and $YBa_2Cu_3O_7$ in the upper part of the figure.

DETERMINATION OF THE STATES INDUCED BY DOPING AT THE Cu L_3 EDGE

The Case of Strontium Doped La_2CuO_4

In the many body description La_2CuO_4 is expected to be a mixture of $3d^9$ and $3d^{10}\underline{L}$ configuration, like CuO and other divalent copper compounds. [70] The doping by oxygen should induce new states $3d^8$ and $3d^9\underline{L}$, if the hole is created at the Cu or at the oxygen site respectively and $3d^{10}\underline{L}^2$ states if both holes are in the oxygen site. Moreover, a distortion of the structure can induce a variation of the mixing between the $3d^{10}\underline{L}$ and $3d^9$ configuration. Therefore the ground state of $La_{2-x}Sr_xCuO_4$ is expected to be a mixture of the $3d^9$ and $3d^{10}\underline{L}$ configurations for the local clusters $(CuO_4)^{6-}$ and of the $3d^9\underline{L}$, $3d^{10}\underline{L}^2$ and $3d^8$ configurations for the local clusters $(CuO_4)^{5-}$ induced in strontium doped sites. The weight of these configurations depends on their relative energy position and hybridization.

The analysis of both the Cu L_3-edge x-ray absorption and the photoemission spectra

ground state parameters such as the energies to create a d hole (ε_d) and an oxygen hole ($\varepsilon_{\underline{L}}$), as function of T, the hybridization energy in the ground state. This approach can be used also to determine the energy parameters of formal trivalent Cu compound such as $NaCuO_2$ which are described by the mixing of the two-hole configurations $3d^9\underline{L}$, $\underline{L}^2$ and $3d^8$ in the ground state, and to discuss the important role of the two holes Coulomb interaction $U_{c\underline{L}}$ between the core hole c and the ligand hole $\underline{L}$ in the final state and the interaction $U_{d\underline{L}}$ between the d hole and the ligand hole $\underline{L}$.

The ground state energies for the two-hole configurations of the strontium induced states in the superconducting compound La-Sr-Cu-O can be made with the same calculation. It shows that the two hole d-L and c-L Coulomb interaction play an important role both in the energy position of the initial and the final states and that the final states are determined by the $3d^8$ contribution in the initial state, also with an hybridization energy of T=2.2 eV, are too weak (~1%) to be detected experimentally. [71]

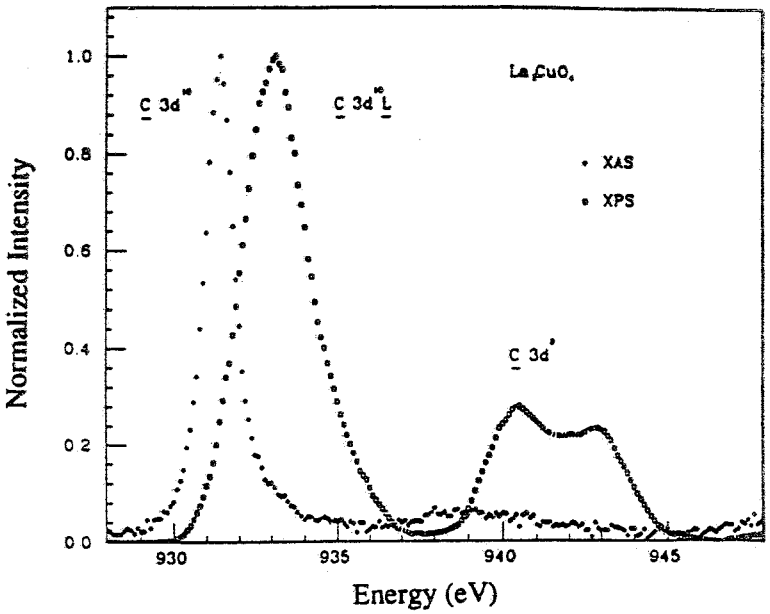

FIG. 9.- Cu L_3-edge XAS and XPS spectra from the Cu $2p_{3/2}$ core level of La_2CuO_4.

In Fig. 9 the Cu L_3 XAS and the Cu $2p_{3/2}$ XPS spectra of La_2CuO_4 are compared on the same energy scale. This compound contains a formal divalent copper and shows a hopping-conductivity behavior but when it is doped with strontium, which induces the increase of the Cu formal valence state, it shows the superconductivity behavior.
The one hole ground state wave function for the divalent copper site is a mixing of the two pure configurations: $|3d^9\rangle$ with one hole on the copper site and $|3d^{10}\underline{L}\rangle$ with one hole on the oxygen site

$$\psi_g = a_g |3d^9\rangle + b_g |3d^{10}\underline{L}\rangle \qquad (15)$$

The $|3d^{10}\underline{L}\rangle$ is the first excited state of the ionic configuration obtained by a charge transfer excitation giving one hole in a 2p orbital. Thus the XAS white line is due to the $\underline{c}3d^{10}$ final state

while the two XPS peaks are due to the hybridization of the two configurations $\underline{c}3d^9$ and $\underline{c}3d^{10}\underline{L}$.

In the frame of this simple orbital model it is possible give an estimation of the final state and ground state energies as a function of the parameters Δ, ε_L, ε_d, Q, U_{cL} and T, where $\Delta=\varepsilon_L-\varepsilon_d$ is the energy to transfer a hole from the copper site to the oxygen site ($\underline{d}\rightarrow\underline{L}$) , ε_L and ε_d are the energies for creating one hole in the oxygen 2p orbital and in the Cu 3d orbital, Q is the $\underline{d}$-$\underline{c}$ hole interaction, T is the hybridization integral between the two configurations ($T=\langle 3d^9|H|3d^{10}\underline{L}\rangle$) and U_{cL} is the pair hole interaction between c and $\underline{L}$ orbital.

Starting from the energy separation between the two XPS peaks: E_2^{XPS} which is the energy of the $\underline{2p}3d^{10}\underline{L}$ main line and E_1^{XPS} which is the energy of the $\underline{2p}3d^9$ satellite line (experimental value $E_2^{XPS}-E_1^{XPS}= 8.5$ eV) and their intensity ratio ($I_2/I_1=0.43$) it is possible the determination of both $Q-U_{cL}$ and Δ as a function of the hybridization T.
ε_L is given by the expression of the energy separation between the XAS main line and XPS main line, which is strongly U_{cL} dependent :

$$E_1^{XPS}-E^{XAS}= \varepsilon_L+U_{cL}+[(Q-U_{cL})-\Delta]/2-\{[(Q-U_{cL})-\Delta]^2+4T^2\}^{1/2}/2 \qquad (16)$$

The introduction in the calculation of the parameter U_{cL}, which determines simply a renormalization of the Q term, reduces the calculated ε_L value and the measured energy separation ($E_1^{XPS}-E^{XAS}=1.8$ eV) becomes mainly a final state effect. The values of ε_L, ε_d and Q, calculated for several values of U_{cL} clearly show that the energy of the ground state, with respect to the energy of the pure copper $3d^{10}$ (Cu^+) oxygen $2p^6$ (O^{2-}) ionic configurations, decreases by increasing the c-L repulsion in the final state. A characteristic set of data obtained by this approach is $\varepsilon_L=1.3$ eV, $\varepsilon_d=0.3$ eV and Q=9.5 eV for $U_{cL}=1.3$ eV and T=2.2 eV).

Formally trivalent copper $NaCuO_2$ compound extends this approach to the case of two holes configurations in the ground state in the XAS final state and to the three holes in the XPS final state. The cluster appropriate for $NaCuO_2$ is a square plane CuO_4 where the diamagnetic ground state is considered to be a singlet pair of two holes given by the linear combination of the $3d^9\underline{L}$, $3d^{10}\underline{L}^2$ and $3d^8$ configurations. The final states are formed by the hybridization of $\underline{c}3d^9\underline{L}$, $\underline{c}3d^{10}\underline{L}^2$ and $\underline{c}3d^8$ for XPS and of $\underline{c}3d^9$, $\underline{c}3d^{10}\underline{L}$ for XAS.

A diagram of the energy levels probed by X-ray photoemission and absorption is shown in Fig. 10 for the trivalent case. The experimental XPS [72] and XAS [73] spectra are shown in Fig. 11, where the white line in the absorption spectrum is due mainly to the $\underline{c}3d^{10}\underline{L}$ and the two XPS peaks come principally from $\underline{c}3d^{10}\underline{L}^2$ and $\underline{c}3d^9\underline{L}$ final states.

The input to extract the energy values of ε_L, ε_d and Q as a function of the pair-hole interactions (U_{dd}, U_{cL}, U_{dL} and U_{LL}) and T, are again the experimental value of the energy separation of the photoemission peaks $E_2^{XPS}-E_1^{XPS}=9.2$ eV, their intensity ratio $I_2/I_1=0.24$, the energy separation between XAS and XPS: $E_1^{XPS}-E_4^{XAS}=1.8$ eV (see Fig. 10) and the effective parameters U_{dd}, U_{cL}, U_{dL} and U_{LL}. With $U_{dd}=8$ eV, chosen in agreement with the experimental valence band photoemission spectra, as in the divalent case, the introduction of hole interactions involving ligand holes reduces in this case both the single-hole energy values and the ground state energy. In Fig. 12 are reported the values Δ, ε_L, ε_d, Q as a function of T, obtained with $U_{cL}=U_{dL}=1.5$ eV and $U_{LL}=0.5$ eV. The energy parameters ε_L and ε_d are lowered respect to the calculation without pair hole interactions U_{cL}, U_{dL} and U_{LL}, giving the values (at T=2.2 eV) of $\varepsilon_L=0.3$ eV, $\varepsilon_d=0.2$ eV and $\Delta=0.1$ eV.

The important result for the trivalent compound is that the cost to create one hole on the ligand orbital is reduced as well as the charge transfer energy Δ. Using these parameters is possible calculate the intensity for the transition at higher energy: about 2% for the XAS and less for the third XPS feature. The XAS and XPS transitions at higher energy named E_5^{XAS} and E_3^{XPS}, due mainly to the $3d^8$ contribution, in fact are not detected experimentally.

The energies of the ground state and of the two excited levels obtained from the hybridization of the ionic configurations $d^{10}\underline{L}^2$ and d^8 are plotted in Fig. 13 as function of the hybridization energy, while Fig. 14 shows the weight of the ionic configurations $3d^9\underline{L}$ (A), $3d^{10}\underline{L}^2$ (B), $3d^8$ (C) in the ground state of $NaCuO_2$. The contribution of the $3d^9\underline{L}$ and $3d^{10}\underline{L}^2$ is nearly the same while the weight of the $3d^8$ is only about 4%.

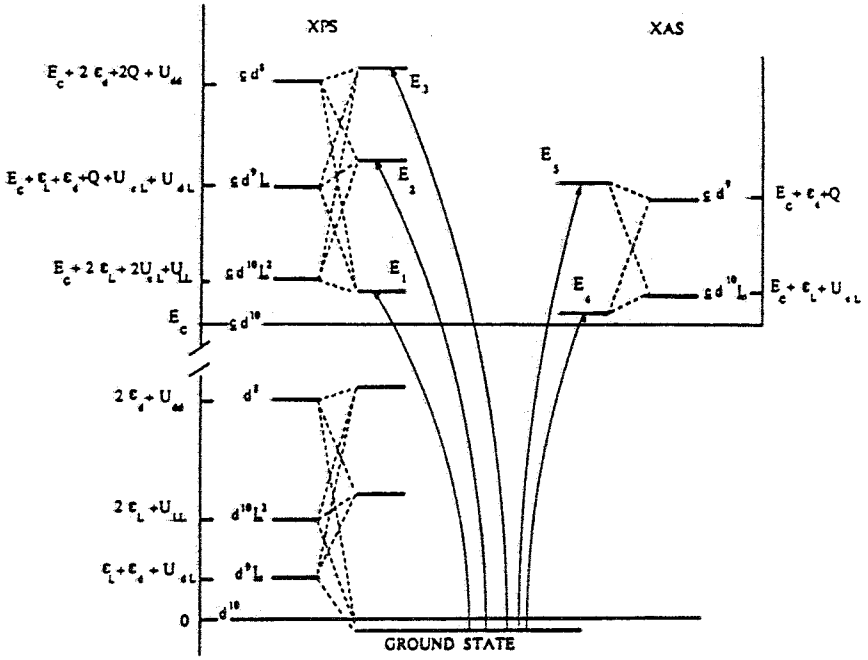

FIG. 10.- Schematic view of the energy levels of the ground state configurations (lower part) and of the excited states for XPS and XAS for the trivalent copper compound $NaCuO_2$.

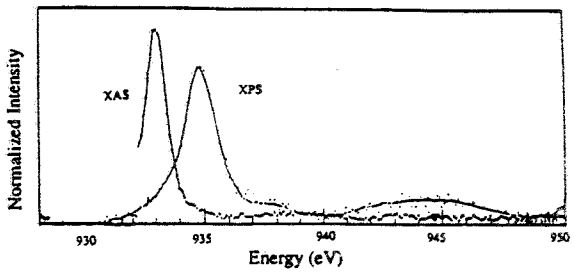

FIG. 11.- L_3-edge x-ray absorption and x-ray photoemission spectra of $NaCuO_2$

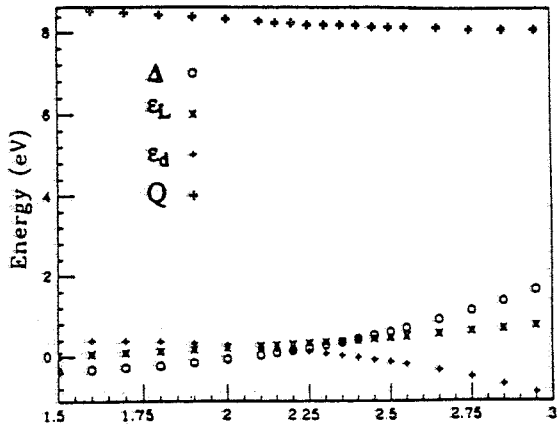

FIG 12.- Variation of the energy parameters Q, Δ, ε_L, ε_d as function of the hybridization energy T in the case of formally trivalent $NaCuO_2$.

For doped La-Sr-Cu-O superconductor with formally mixed copper valence the ground state is a superposition of the nominally divalent Cu with one-hole states $3d^9$ and $3d^{10}\underline{L}$, and nominally trivalent Cu with two-hole states $3d^8$, $3d^9\underline{L}$, and $3d^{10}\underline{L}^2$ states. Although extra holes move around and are not localized in actual systems the ground state is constructed by hybridization of the one-hole and two-hole configurations. However, neglecting at first approximation the mixing between divalent and trivalent configuration, by subtracting the La_2CuO_4 spectra to the superconductor ones a simulation of the spectra of a "trivalent" compound could be obtained. In Fig.15 the differences between the L_3 core level XAS and $2p_{3/2}$ XPS spectra of the superconducting compound $La_{1.15}CuO_4$ and La_2CuO_4 are plotted. Similar experimental results are obtained for the differences of XPS spectra of Y-Ba-Cu-O system. [72]

Similar analysis of $NaCuO_2$ can be carried out on these difference spectra using the experimental values of E_2^{XPS}-E_1^{XPS}=8.1 eV, I_2/I_1=0.3 and E_1^{XPS}-E_4^{XAS}=2.1 eV, which gives the curves reported in Fig.16. The ε_L, ε_d, Δ and Q curves are obtained for parameters values of U_{cL}=U_{dL}=1.3 eV and U_{LL}=0.8 eV (U_{dd}=8 eV) with T=2.2 eV obtaining now the values of ε_L=0.5 eV, ε_d=0 eV and Δ=0.5 eV.

The energy values of the three hybridized states for the two hole states are reported in Fig. 17. The configuration F1 is the ground state. The excited configuration F3 at the highest energy is mainly due to the $3d^8$ configuration. Its energy is calculated to be at about 9 eV above the energy of the pure copper $3d^{10}$ (Cu^+) oxygen $2p^6$ (O^{2-}) ionic configurations. The contribution of the $3d^8$ configuration to the ground state (Fig. 18) is of the order of 6%.

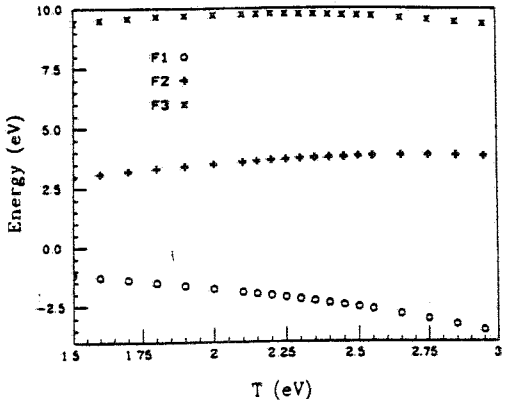

FIG. 13.- Energies of the ground state (F1) and of the two excited levels F2*and F3 obtained from the hybridization of the ionic configuration $d^{10}\underline{L}^2$ and d^8 as a function of the hybridization energy T for the formally trivalent compound $NaCuO_2$.

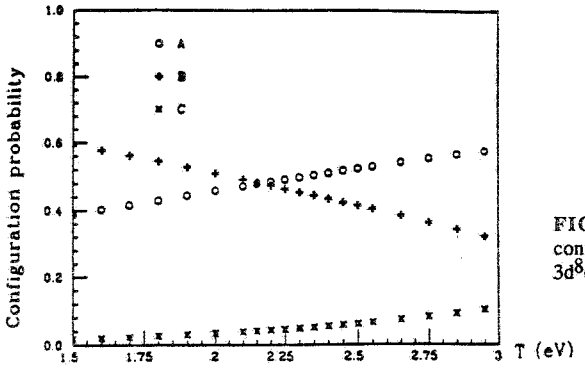

FIG. 14.- Weight of the ionic configurations $3d^9\underline{L}$(A), $3d^{10}\underline{L}^2$(B) and $3d^8$(C) in the ground state of $NaCuO_2$.

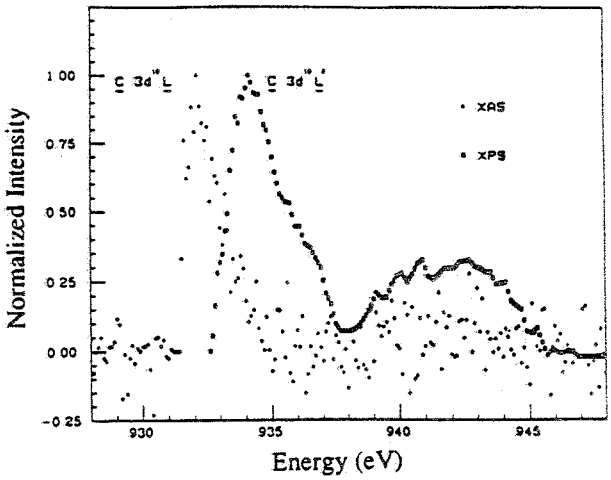

FIG. 15.- Difference between the L_3 XAS and Cu $2p_{3/2}$ XPS spectra of $La_{1.85}Sr_{0.15}CuO_4$ and La_2CuO_4.

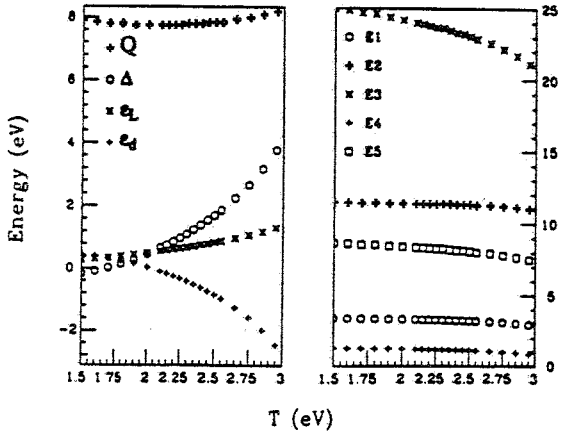

FIG. 16.- *Left panel*: variation of the energy parameters Q, Δ, $\varepsilon_{\underline{L}}$ and ε_d as a function of the hybridization energy T for the two hole states induced by doping. These curves were found by considering the difference of the XPS and XAS spectra shown in Fig. 15 between the superconducting compound $La_{1.85}Sr_{0.15}CuO_4$ and the divalent one La_2CuO_4. *Right panel*: XAS and XPS final state energies. The E3 and E5 transition not observed in the experiment are obtained using as imput the experimental E1, E2 and E4 values and the parameters in left side panel.

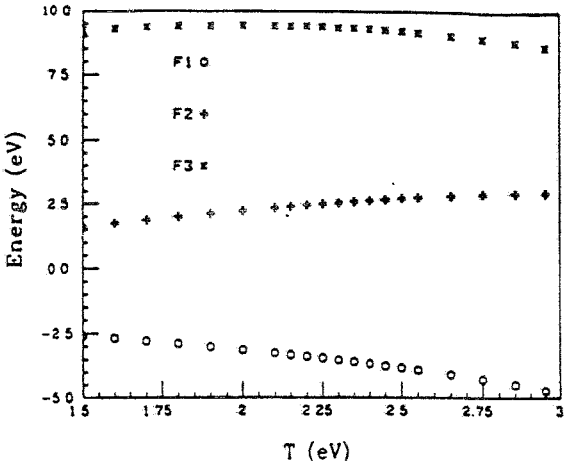

FIG. 17 - Energies of the ground state (F1) and of the two excited levels (F2 and F3) obtained by the hybridization of the ionic configuration $d^{10}\underline{L}^2$ and d^8 as a function of the hybridization energy T for the two hole states induced by doping in the superconducting compound $La_{1.85}Sr_{0.15}CuO_4$.

CORRELATION BETWEEN T_c AND THE ENERGY SPLITTING OF POLARIZED Cu 2p->3d TRANSITION

Sr doping in La_2CuO_4 system or oxygen doping in $YBa_2Cu_3O_{6.5+x}$ show the formation of $3d^9\underline{L}$ states at the copper L_3 X-ray absorption spectra. These states are due to many body configuration with itinerant holes in the oxygen valence band coupled with localized 3d electrons on the Cu sites which are close to the Fermi level in the superconducting phase. A key point in a deeper investigation of the electronic structure is the determination of the changes of unoccupied states induced by oxygen doping in the antiferromagnetic insulating background.

High resolution polarized Cu L_3 x-ray absorption spectra of single crystals of three classes of high temperature superconductors $La_{2-x}Sr_xCuO_4$ (x=0.04 and x=0.1) $Bi_2CaSr_2Cu_2O_8$ and $YBa_2Cu_3O_{6-\delta}$ have been measured in order to determine via the different direction of the polarization vector where extra holes exist in a high temperature oxide superconductors.

Polarized spectra of single crystals with several incidence angles between the electric field of the photon beam **E** and the sample surface normal **z** can be simply recorded, using synchrotron radiation linearly polarized in the horizontal plane. [74]
For the case of $Bi_2Sr_2Ca_1Cu_2O_8$ and $YBa_2Cu_3O_{7-\delta}$ the **z** axis is parallel to the **c** axis while for $La_{2-x}Sr_xCuO_{4-y}$ the **z** axis is parallel to the **b** axis. The full polarized XAS spectra (**E**⊥**z**) (**E** parallel to the **xy** plane of the CuO_2 layers) and (**E**∥**z**) can be obtained by extrapolation of the spectra taken at four different incidence angles. The study of the polarization dependence of the "white line" in the Cu L_3-edge XAS due to $2p_{3/2}$->3d transition in the antiferromagnetic insulating La_2CuO_4 and superconducting crystals of $La_{2-x}Sr_xCuO_4$ (x=0.04 and x=0.1), $Bi_2CaSr_2Cu_2O_8$ and $YBa_2Cu_3O_{7-\delta}$ (δ=4.5 and δ=0.2) shows the presence of the electronic transition polarized in the **z** direction which probe the components of the orbitals of the d holes in the **z** direction. [75] The investigation of the energy splitting $\Delta\varepsilon$ between the in-plane and out-plane 2p->3d transition shows that the splitting for each class of superconductors is correlated with the critical temperature of the superconducting crystals.

While it is well established that the holes induced by doping are mainly in the oxygen derived valence band i.e. ligand holes giving the $3d^9\underline{L}$ configuration, [28,30,71,76-78] the determination of the symmetry of the two holes states found by photoinduced IR [79] and by many other methods is still an open problem.

As is well known, the 5 Cu 3d orbitals are splitted by the crystalline field with D_{4h} symmetry into four energy levels: the b_1 (x^2-y^2) orbital which corresponds to the highest level, the a_1 ($3z^2$-r^2) orbital, the b_2 (xy) orbital and e (d_{xz},d_{yz}) orbitals. The ligand hole $\underline{L}$ wave functions consist of linear combinations of oxygen 2p orbitals with the above symmetries.
The electronic configuration of the Cu ions in the antiferromagnetic insulating compounds is expected to be the Cu $3d^9$ configuration, where the d hole is in the Cu $3d_{x^2-y^2}$ orbital of b_1 molecular symmetry in the CuO_4 square plane cluster. This is expected for a perfect square plane but it is well known that a simple system of regular CuO_4 square plane does not exhibit high temperature superconductivity above 20 K.
The tilting of the elongated octahedron of the $La_{2-x}Sr_xCuO_4$ and the distortions of the CuO_5 square pyramids of $Bi_2CaSr_2Cu_2O_8$ and $YBa_2Cu_3O_{7-\delta}$ induces a mixture of $3d_{3z^2-r^2}$ symmetry (a_1 molecular symmetry) or of the $3d_{xz}$ (e molecular symmetry) with the $3d_{3z^2-r^2}$ in the ground state. [80,81]
There are several experimental indications that the holes are not present only in the upper valence band σ bond formed by the $3d_{x^2-y^2}$ and the $O(2p_x)$ or $O(2p_y)$ in the CuO_2 layers. The holes induced by doping in $YBa_2Cu_3O_{7-\delta}$ (T_c=80K system) are present in the apical oxygen O(4) of Cu(2) which is also in the linear Cu(1)O chains.[74,78].
Evidence for d-d excitations in $YBa_2Cu_3O_7$ has been also reported, [82] and the study of the polarization dependence of the "white line" in the Cu L_3-edge XAS of $Bi_2CaSr_2Cu_2O_8$ has also indicated the presence of 10%-20% of Cu 3d holes oriented in the z direction. [75,83]

Several theoretical models for high T_c superconductivity such as the three band model [84,85] the spin polaron pairing mechanism [86] the d-d excitation model, [87-90] the Kanamori model [91] and the interlayer pairing [92-94] require the presence of electronic states with two holes in two different orbitals.

Fig. 19 shows the white line due to Cu 2p->3d transitions of the polarized, E||z and E⊥z, Cu L_3 XAS of the insulating La_2CuO_{4-y} and of superconducting $La_{1.96}Sr_{0.04}CuO_4$ and $La_{1.9}Sr_{0.1}CuO_4$. The curves in Fig. 19 are normalized to the white line maximum to show the energy shift. The white line maximum for the E||z polarization is always at lower energy than for the E⊥z polarization. The energy separation $\Delta\varepsilon$ between the maxima of the two polarized white lines can be obtained by curve fitting avoiding the artifact of the variation of the lineshape with the incidence angle. The energy separation $\Delta\varepsilon$ decreases from 230 ± 50 meV to 80 ± 50 meV going from La_2CuO_{4-y} to $La_{1.9}Sr_{0.1}CuO_4$. The intensity of the E||z white line is about 25% of the intensity of the E⊥z white line with an error in the measure of the relative intensity of about 15-20%. The presence of a small component of the white line for E||z polarization indicates that there are Cu d holes having a component of their orbital in the z direction $\underline{d_z}$ ($\underline{d_z}$ is introduced here to indicate one of the three possible 3d orbital: $3d_{3z^2-r^2}$, d_{xz} or d_{yz} that this experiment cannot separate).

Fig. 20. reports the polarized Cu L_3-edge XAS of $YBa_2Cu_3O_{6.5}$ (T_c=60K), b) $YBa_2Cu_3O_{6.8}$ (T_c=82.5K) in a larger energy range including the white line and the shoulder at about 1.5 eV above it. The energy separation $\Delta\varepsilon$ between the white lines in the two polarizations decreases from 200 meV to 120 meV going from T_c=60K to T_c=82.5K sample.

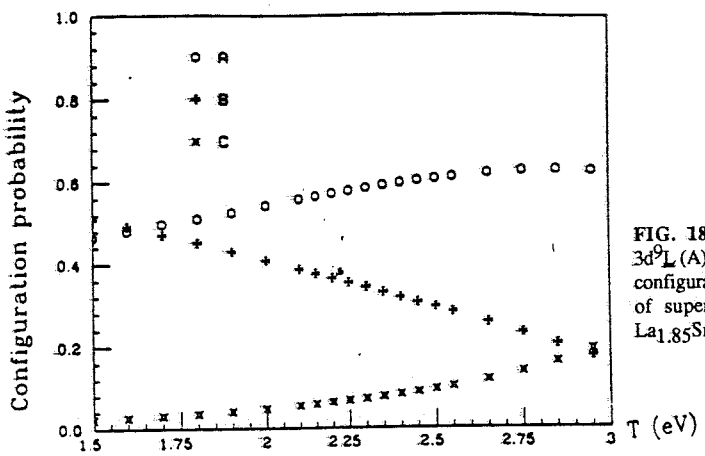

FIG. 18 - Weight of the ionic $3d^9\underline{L}$ (A), $3d^{10}\underline{L}^2$ (B) and $3d^8$ (C) configurations in the ground state of superconducting compound $La_{1.85}Sr_{0.15}CuO_4$.

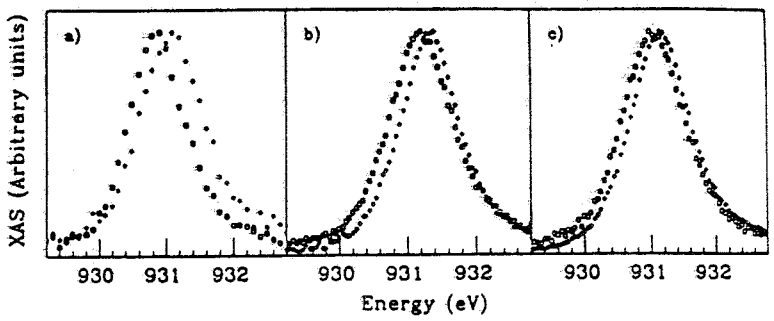

FIG. 19 - Polarized L_3-edge XAS spectra measured with electrical field parallel (E||z) (□) and perpendicular (E⊥z) (◇) to the sample z axis, for: a) La_2CuO_{4-y} , b) $La_{1.96}Sr_{0.04}CuO_4$, and c) $La_{1.9}Sr_{0.1}CuO_4$

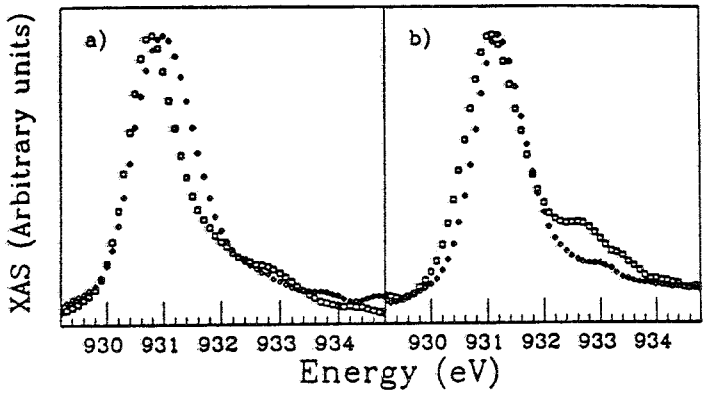

FIG. 20 - Polarized L$_3$-edge XAS spectra measured with electrical field parallel (E||z) (□) and perpendicular

In Fig. 21 the white lines of polarized Cu L_3-edge XAS of a highly oriented film $Bi_2Sr_2Ca_1Cu_2O_y$, (T_c=61K) with incidence angle ϕ=10° and 75° are shown. [83] The spectra of a CuO polycristalline sample of the same size have been recorded in the same run in order to keep under control the energy calibration and any other possible effects on the data collection. The CuO spectra do not change by changing the angle of incidence while the white line of $Bi_2Sr_2Ca_1Cu_2O_y$ film shows a large anisotropy. This data show that the white line has two components separated by an energy splitting $\Delta\varepsilon$ of about 400 eV. The peak B at higher energy observed for the polarization direction E⊥c is interpreted as an evidence for the presence of d holes with $3d_{3z^2-r^2}$ simmetry.

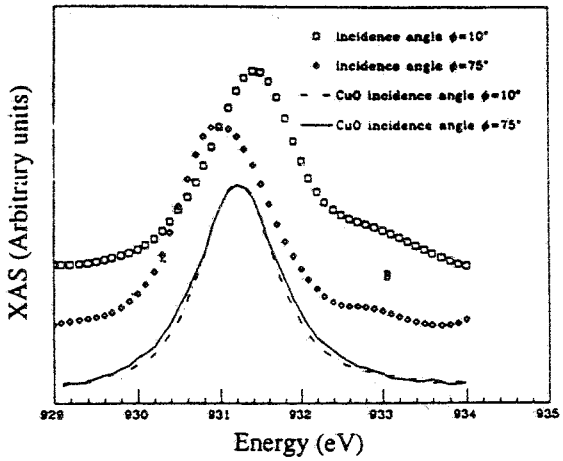

FIG. 21 - Polarized Cu L_3-edge XAS spectra for $Bi_2Sr_2Ca_1Cu_2O_y$ oriented film (T_c=61K) for two extreme incidence angles ϕ=10°, i.e. with the electric field nearly parallel to the CuO_2 planes (E⊥c)(□), and for ϕ=75°, with the electric field nearly normal to the CuO_2 planes (E||c)(◇).

Fig. 22 reports the energy difference $\Delta\varepsilon$ between the maximum of the in-plane (the **xy** plane of CuO_2 layers) E⊥**z** polarized white line and the out-of-plane E||**z** polarized line for the three classes of compounds as function of the critical temperature of each sample.
In the series of $La_{2-x}Sr_xCuO_4$ the values of $\Delta\varepsilon$ reaches its maximum for the insulating x=0 system. These results show that the doping induces an important change in the d unoccupied states by reducing the energy separation between the unoccupied states with components along **z** and that with components along the **xy** plane.

Bianconi *et al.* [30] in order to discuss the problem of the symmetry of the $3d^9\underline{L}$ states in the doped $La_{2-x}Sr_xCuO_4$, have shown that the $3d^9\underline{L}$ states induced by doping gives an high energy tail of the white line of unpolarized La_2CuO_4. The difference between the E⊥c spectra of $La_{2-x}Sr_xCuO_4$ for x=0.04 minus x=0.10, recorded under the same experimental conditions and with the same instrumental broadening, is reported in Fig. 23. While no detectable variation are found in the difference between the E||c spectra, the spectrum of the difference is similar to that of the unpolarized spectra, [30] therefore the states induced by doping in the low T_c regime (T_c=12K) are mainly $\underline{d}_x\underline{L}$. From the results of De Sanctis *et al.* [71] the observed shoulder can be associated with the formation of singlet states $\underline{d}(b_1)\underline{L}(b_1)$ with $U_{d\underline{L}}$=1.3 eV, therefore both $La_{2-x}Sr_xCu_2O_4$ (x=0.1) and $Bi_2Sr_2CaCu_2O_8$ [83] crystals show the presence of a resolved shoulder $\underline{2p}3d^{10}\underline{L}$ in the range 1-2 eV above the white line for the E⊥z polarization indicating the presence of $\underline{d}(b_1)\underline{L}(b_1)$ states.

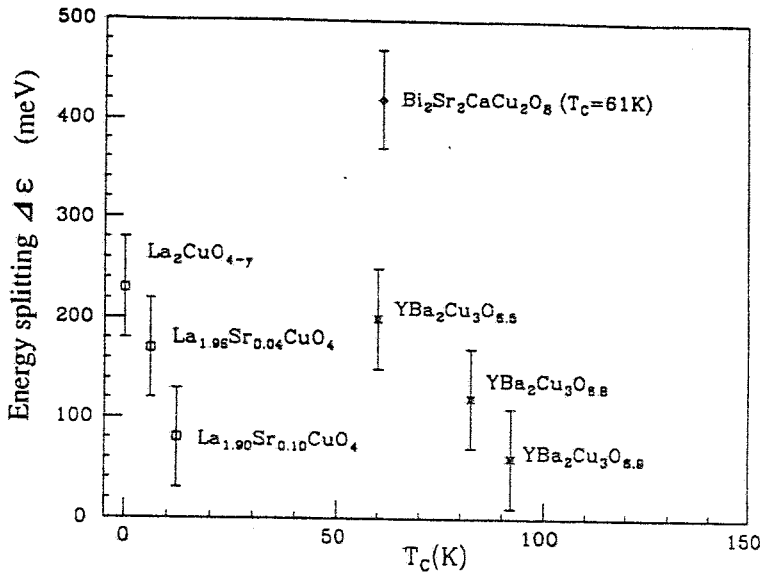

FIG. 22 - Energy splitting between the peaks of polarized white lines in the L_3-edge XAS (E⊥c peak minus E∥c peak) as function of critical temperature (T_c) for the following classes of superconductors: $La_{2-x}Sr_xCu_2O_4$ (□), $YBa_2Cu_3O_{7-\delta}$ (+), and $Bi_2Sr_2CaCu_2O_8$ (◇).

The triplet states $\underline{d}(a_1)\underline{L}(b_1)$ are not detected by the Cu L_3 XAS spectroscopy because the split-off of the shoulder from the energy region of the white line is determined by the Coulomb repulsion $U_{cL} \sim U_{dL}$ which for the $\underline{d}(a_1)\underline{L}(b_1)$ is expected to be much smaller than 1.3 eV for $\underline{d}(b_1)\underline{L}(b_1)$. [87-90] Because of the small value of U_{cL}, the final states determined by $\underline{d}(a_1)\underline{L}(b_1)$ configuration are expected to be unresolved from the E∥z white line. The presence of the white line component E∥z indicates the possible presence of the $\underline{d}(a_1)\underline{L}(b_1)$ or $\underline{d}(e)\underline{L}(b_1)$ configurations with $U_{cL} \sim U_{dL}$ smaller than 1 eV. In fact the $\underline{L}(b_1)$ was detected by oxygen K-edge absorption of $Bi_2Sr_2CaCu_2O_8$ by Fink *et al.* [77] and the holes $\underline{d}_z$ with Cu 3d orbital components in the z direction ($\underline{d}_z$ indicates one of the 3d orbital: $3\underline{d}_{3z^2-r^2}$ (a_1) or $\underline{d}_{xz}$, $\underline{d}_{yz}$ (e)) are detected by the polarization dependence of the L_3 XAS white line.

The presence of the holes out of the CuO_2 plane is found in the high T_c range of the $YBa_2Cu_3O_{7-\delta}$ system. Moreover the shoulder at 1.5 eV above the white line in Fig. 20 is much weaker in the spectrum of the T_c=60K sample than in the spectrum of the T_c=82.5K sample. [74] The E⊥z spectrum of the T_c=60K sample shows an asymmetric high energy tail of the white line indicating the presence of a $3d^9\underline{L}$ configuration with $\underline{d}$ unoccupied orbital $\underline{d}_x\underline{L}$ in the CuO_2 plane. Most of the weight of the 1.5 eV shoulder observed in the E∥z spectra of the T_c~80K is formed with the transition from the low T_c range (50-60K) to the high T_c range (80-90K). Taking into account that the presence of the hole in the apical O(4) is detected by the analysis of the x-ray absorption at the Cu(1) ions, these results are in agreement with the theoretical prediction of Fujimori, [95] which shows that the ligand hole is stabilized in the apical oxygen by decreasing the Cu(2)O(4) distance. Therefore for 50-60K superconductivity both $\underline{d}_x\underline{L}$ and $\underline{d}_z\underline{L}$ configuration have comparable probability while in the 80-90K superconductivity the holes are found to be mostly out of the CuO_2 plane.

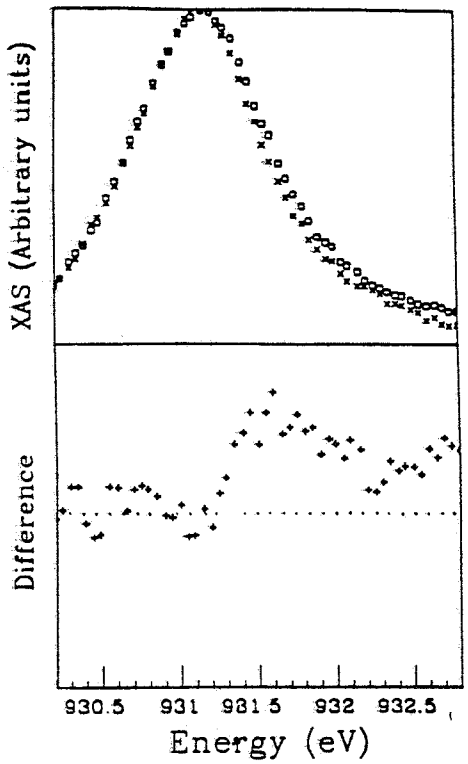

FIG. 23 - Comparison between the white lines of L_3-edge XAS spectra measured with an angle of 80^o between the photon electric field **E** and the z axis of $La_{2-x}Sr_xCu_2O_4$ x=0.04 (+) and x=0.1 (□). In the lower panel the difference between the two spectra is plotted to show the spectrum of strontium induced transitions with a peak at about 931.7 eV. The dotted line indicates the zero of the difference.

SUMMARY

Joint analysis of XPS and XAS spectra of the same core level is a simple experimental approach to obtain the energies of the two hole configurations in a formally trivalent compound and for the states induced by doping in superconductor systems like $La_{1.85}Sr_{0.15}CuO_4$. Without neglect the limitations of this simple approach which does not consider the multiplet splitting, the bandwidth, and takes in consideration only one type of orbital symmetry for the d and L holes it shows that in the copper-oxygen compounds the pair-hole interaction in the final state U_{cL}, strongly affects the energy difference between the x-ray absorption (XAS) and the x-ray photoemission (XPS) main lines, and the pair-hole interactions U_{dL} and U_{LL} both in the ground state and in the final state are important to calculate the energies of the two holes ground state.

There is evidence from polarized L_3 XAS spectroscopy of a correlation between the critical temperature of a superconductors and the energy splitting of the **E**⊥z and **E**∥z polarized "white lines" in agreement with the predictions of the d-d excitation model. [87-90]. The expected formation of singlet states $\underline{d}(b_1)\underline{L}(b_1)$ states have been found but $\underline{d}_z$ holes are also present. In particular in the $YBa_2Cu_3O_7$ system for the higher critical temperature there is evidence of oxygen induced ligand hole out of the CuO_2 planes. The intensity of the $\underline{d}(b_1)\underline{L}(b_1)$ is expected to decrease with the decrease of the ratio between $d_{x^2-y^2}$ and d_z states over the U_{cL} interaction. On the contrary the configurations $d(a_1)\underline{L}(b_1)$ [87-90] or $d(b_1)\underline{L}(a_1)$, where the

Acknowledgements

I gratefully acknowledge Prof. A. Bianconi who involved me in the study of high-temperature superconductivity and for his encouraging support in all these years. A special thank to A. Kotani for many stimulating discussion and to A.M. Flank, A. Fontaine and P. Lagarde for their invaluable support. I have also benefited from the close collaboration with many colleagues, especially P. Castrucci, A. Clozza, M. De Santis, S. Della Longa, M. De Simone, A. Di Cicco, A. Fabrizi, A. Gargano and M. Pompa.

REFERENCES

[1] C. Michel and B. Raveau, J. Solid State Chem. 43, (1982) 73.
[2] C. Michel and B. Raveau, Rev. Cim. Mineral., 21, (1984) 407.
[3] C. Michel, L. Er-Rakho and B. Raveau, Mater. Res. Bull. 20, (1985) 667.
[4] J.C. Bednorz and K.A. Müller, Z. Phys. B - Condensed Matter 64, (1986) 189.
[5] J.C. Bednorz, M. Takashige and K.A. Müller, Europhys. Lett. 3, (1987) 379.
[6] K. Okada and A. Kotani, J. Phys. Soc. Japan 58, (1989) 1095.
[7] A. Fujimori, E. Takayama-Muromachi, Y. Uchida and B. Okai, Phys. Rev. B 35, (1987) 8814.
[8] A. Fujimori, E. Takayama-Muromachi and Y. Uchida, Solid State Commun. 63, (1987) 857.
[9] A. Bianconi, A. Congiu Castellano, M. De Santis, P. Delogu, A. Gargano and R. Giorgi, Solid State Commun. 63, (1987) 1135.
[10] Z. Shen, J.W. Allen, J.J. Yeh, J.-S. Kang, W. Ellis, W. Spicer, I. Lindau, M.B. Maple, Y.D. Dalichaouch, M.S. Torikachvili, J.S. Sun and F. Geballe, Phys. Rev. B 36, (1987) 8414.
[11] P. Steiner, S. Hufner, V. Kinsinger, I. Sander, B. Siegwart, H. Schmitt, R. Schulz, S. Junk, G. Schwitzgebel, A. Gold, C. Politis, H.P. Muller, R. Hoppe, S. Kemmeler-Sack and C. Kunz, Z Phys. B - Condensed Matter 69, (1988) 449.
[12] G. Gourieux, G. Krill, M. Maurer, M.F. Ravet, A. Menny, H. Tolentino and A. Fontaine, Phys. Rev. B 37, (1988) 7516.
[13] R. Kurtz, R.L. Stochbauer, D. Mueller, A. Shih, L.E Toth, M. Osofsky and S.A. Wolf, Phys. Rev. B 35, (1987) 8818.
[14] M. Onellion, Y. Chang, D.W. Niles, R. Joynt, G. Margaritondo, N.G. Stoffel and J.M. Tarascon, Phys. Rev. B 36, (1987) 819.
[15] J.A. Yarmoff, D.R. Clark, W. Drube, U.O. Karlsson, A. Taleb-Ibrahimi and F.J. Himpsel, Phys. Rev. B 36, (1987) 3967.
[16] N.G. Stoffel, J.M. Tarascon,Y. Chang, M. Onellion, D.W. Niles and G. Margaritondo, Phys. Rev. B 36, (1987) 3986.
[17] T. Takahashi, F. Maeda, H. Arai, H. Katayama-Yoshida, Y. Okabe, T. Suzuki, S. Hosoya, A. Fujimori, T. Shidara, T. Koide, T. Miyahara, M. Onoda, S. Shamoto and M. Sato, Phys. Rev. B 36, (1987) 5686.
[18] J. Zaanen, G.A. Sawatzky and J.W. Allen, Phys. Rev. Lett. 55, (1985) 418.
[19] P.Steiner, J. Albers, V. Kinsinger, I. Sander, B. Siegwart, S. Hufner and C. Politis, Z. Physik B - Condensed Matter 66, (1987) 275.
[20] N. Nucker, J. Fink, B. Renker, D. Ewert, C. Politis, P.J.W. Weijs and J.C. Fuggle, Z. Phys. B - Condensed Matter 67, (1987) 9.
[21] T. Takahashi, F. Maeda, H. Katayama-Yoshida, Y. Okabe, T. Suzuki, A. Fujimori, S. Hosoya, S. Shamoto and M. Sato, Phys. Rev. B 37, (1988) 9788.
[22] J.M. Tranquada, S.M. Heald, A. Moodenbaugh and M. Suenaga, Phys. Rev. B 35, (1987) 7187.
[23] E.E. Alp, G.K. Shenoy, D.G. Hinks, D.W. Capone II, L. Soderholm, H.B. Schuttler, J. Guo, D.E. Ellis, P.A. Montano and M. Ramanathan, Phys. Rev. B 35, (1987) 7199.
[24] [illegible]

[25] H. Oyanagi, H. Ihara, T. Matsubara, T. Matsushita, M. Hirabayashi, M.Tokumoto, K. Murata, N. Terada, K. Senzaki, T. Yao, H. Iwasaki and Y. Kimura, Jpn. Journ. Appl. Phys. 26, (1987) L1233 and ibidem 26, (1987) L638.
[26] A. Bianconi, A. Congiu Castellano, M. De Santis, C. Politis, A. Marcelli, S. Mobilio and A. Savoia, Z. Physik B - Condensed Matter 67, (1987) 307.
[27] F. Baudelet, G. Collin, E. Dartyge, A. Fontaine, J.P. Kappler, G. Krill, J.P. Itié, J. Jegoudez, M. Maurer, Ph. Monod, A. Revcolevschi, H. Tolentino, G. Tourillon and M. Verdaguer, Z. Physik B - Condensed Matter 69, (1987) 141.
[28] A. Bianconi, A. Congiu Castellano, M. De Santis, P. Rudolf, P. Lagarde, A.M. Flank and A. Marcelli, Solid State Commun. 63, (1987) 1009.
[29] A. Bianconi, A. Clozza, A. Congiu Castellano, S. Della Longa, M. De Santis, A. Di Cicco, K. Garg, P. Delogu, A. Gargano, R. Giorgi, P. Lagarde, A. M. Flank and A. Marcelli, Int. J. Modern Phys. B 1, (1987) 853.
[30] A. Bianconi, J. Budnick, A.M. Flank, A. Fontaine, P. Lagarde, A. Marcelli, H. Tolentino, B. Chamberland, C. Michel, B. Raveau and G. Demazeau, Phys. Lett. A 127, (1988) 285.
[31] A. Bianconi, M. De Santis, A. Clozza, A. Congiu Castellano, A.M. Flank, A. Fontaine, P. Lagarde, J. Budnick and A. Gargano, Core Level Spectroscopy in Condensed Systems, (Eds.J. Kanamori and A. Kotani), Springer Verlag, Berlin, (1988), pp. 146.
[32] U. Fano and J.W. Cooper, Rev. Mod. Phys. 40, (1968) 441.
[33] J.E. Müller, O. Jepsen and J.W. Wilkins, Solid State Commun. 42, (1982) 365.
[34] J.E. Müller and J.W. Wilkins, Phys. Rev. B 29, (1984) 4331.
[35] J. Fink, Th. Müller-Heinzerling, B. Scheerer, W. Speier, F.U. Hillebrecht, J.C. Fuggle, J. Zaanen and G.A. Sawatzki, Phys. Rev. B 32, (1985) 4899.
[36] J. Zaanen, G.A. Sawatzki, J. Fink, W. Speier and J.C. Fuggle, Phys. Rev. B 32, (1985) 4905.
[37] G.A. Sawatzki, Core Level Spectroscopy in Condensed Systems, (Eds.J. Kanamori and A. Kotani), Springer Verlag, Berlin, (1988), pp.99 and reference therein.
[38] U. von Barth and G. Grossmann, Solid State Commun. 32, (1979) 645.
[39] U. von Barth and G. Grossmann, Phys. Rev. B 25, (1982) 5150.
[40] A. Kotani, T. Jo and J. C. Parlebas, Adv. Phys. 37, (1988) 37.
[41] A. Bianconi, A. Kotani, K. Okada, R. Giorgi, A. Gargano, A. Marcelli and T. Miyahara, Phys. Rev. B 38, (1988) 3433.
[42] A. Bianconi, T. Miyahara, A. Kotani, Y. Kitajima, T. Yokoyama, H. Kuroda, M. Funabashi, H. Arai and T. Ohta, Phys. Rev. B 39, (1989) 3380.
[43] M. Piacentini, EXAFS and Near Edge Structure, (Eds. A. Bianconi, L. Incoccia and S. Stipcich), Springer Verlag, Berlin, (1983), pp.193.
[44] D.H. Templeton and L.K. Templeton, Acta Crystallogr. A38, (1982) 62.
[45] J.E. Penner-Hahn, R.A. Scott, K.O. Hodgson, S. Doniach, S.R. Desjardins and E.I. Solomon, Chem. Phys. Lett. 88, (1982) 595.
[46] T.A. Smith, J.E. Penner-Hahn, M.A. Berding, S. Doniach and K.O. Hodgson, J. Am. Chem. Soc. 107, (1985) 5945.
[47] N. Kosugi, T. Yokoyama, K. Asakura and H. Kuroda, Chem. Phys. 91, (1984) 249.
[48] F.W. Kutzler, R.A. Scott, J.M. Berg, K.O. Hodgson, S. Doniach, S.P. Cramer and C.H. Chang, J. Am. Chem. Soc. 103, (1981) 6083.
[49] A. Bianconi, A. Congiu Castellano, P.J. Durham, S.S. Hasnain and S. Phillips, Nature 318, (1985) 685.
[50] R.A. Scott, J. Penner-Hahn, S. Doniach, H.C. Freeman and K.O. Hodgson, J.Am. Chem. Soc. 104, (1982) 5364.
[51] S. Stizza, M. Benfatto, I. Davoli, G. Mancini, A. Marcelli, A. Bianconi, M. Tomellini and J. Garcia, J. Physique 46, C8, (1985) 255
[52] S. Stizza, M. Benfatto, J. Garcia and A. Bianconi, J. Physique 47, C8, (1986) 691.
[53] J.E. Penner-Hahn, M. Benfatto, B. Hedman, T. Takahashi, S. Doniach, J.T. Groves and K.O. Hodgson, Inorg. Chem. 25, (1986) 2255.
[54] P.A. Lee, Phys. Rev. B 13, (1976) 5261.
[55] S.M. Heald and E.A. Stern, Phys. Rev. B 17, (1978) 4069.

[56] J. Stöhr, X-ray Absorption: Principles and Techniques of EXAFS, SEXAFS and XANES, (Eds. R. Prinz and D. Konigsberger), Wiley, New York, (1986).
[57] J. Stöhr and R. Jaeger, Phys. Rev. B 26, (1982) 4111.
[58] J. Stöhr, J.L. Gland, E.B. Kollin, R.J. Koestner, A.L. Johnson, E.L. Muetterties and F. Sette, Phys. Rev. Lett. 53, (1984) 2161.
[59] T. Iwazumi, I. Nakai, M. Izumi, H. Oyanagi, H. Sawada, H. Ikeda, Y. Saito, Y. Abe, K. Takita and R. Yoshizaki, Solid State Commun. 65, (1988) 213.
[60] H. Oyanagi, H. Ihara, T. Matsubara, T. Matsushita, M. Hirabayashi, M. Tokumoto, K. Murata, N. Terada, K. Senzaki, T. Yao, H. Iwasaki and Y. Kimura, Jpn. Journ. Appl. Phys. 26, (1987) L1233.
[61] J.M. Tranquada, S.M. Heald, A.R. Moodenbaugh and Y. Xu, Phys. Rev. B 38, (1988) 8893.
[62] H. Tolentino, E. Dartyge, A. Fontaine, G. Tourillon, T. Gourieux, G. Krill, M. Maurer and M.F. Ravet, High T_c Superconductors: Electronic Structure, (Eds. A. Bianconi and A. Marcelli), Pergamon Press, Oxford, (1989).
[63] E.E Alp, S.M. Mini, M. Ramanathan, B.W. Veal, L. Soderholm, G.L. Goodman, B. Dabrowski, G.K. Shenoy, A. Bommanavar and O.B. Hyun, (1989) to be published
[64] G. Onori, A. Santucci, A. Scafati, M. Belli, S. Della Longa, A. Bianconi and L. Palladino, Chem. Phys. Lett. 149, (1988) 289.
[65] R.J. Cava, B. Batlogg, S.A. Sunshine, T. Siegrist, R.M. Fleming, K. Rabe, L.F. Schneemeyer, D.W. Murphy, R.B. van Dover, P.K.Gallagher, S.H. Glarum, S. Nakahara, R.C. Farrow, J.J. Krajewski, S. M. Zahurak, J.V. Waszczak, J.H. Marshall, P. Marsh, L.W. Rupp, Jr. W.F. Peck and E.A. Rietman, Physica C 153-154, (1988) 560.
[66] S. Della Longa, M. De Simone, C. Li, M. Pompa and A. Bianconi, High T_c Superconductors: Electronic Structure, (Eds. A. Bianconi and A. Marcelli), Pergamon Press, Oxford, (1989).
[67] K.B. Garg, A. Bianconi, S. Della Longa, A. Clozza, and M. De Santis and A. Marcelli, Phys. Rev. B 38, (1987) 244.
[68] S.M. Heald, J.M. Tranquada, A.R. Moodenbaugh and Y. Xu, Phys. Rev. B 38, (1988) 761.
[69] A. Bianconi, M. Dell' Ariccia, A. Gargano and C.R. Natoli, EXAFS and Near Edge Structure, (Eds. A. Bianconi, L. Incoccia and.S. Stipcich), Springer Verlag, Berlin, (1983), pp.57.
[70] G. van der Laan, C. Westra, C. Haas and G.A. Sawatzky, Phys. Rev. B 23, (1981) 4369.
[71] M. De Santis, A. Bianconi, A. Clozza, P. Castrucci, A. Di Cicco, M. De Simone, A M. Flank, P. Lagarde, J. Budnick, P. Delogu, A. Gargano, R. Giorgi and T.D. Makris, High T_c Superconductors: Electronic Structure, (Eds. A. Bianconi and A. Marcelli), Pergamon Press, Oxford, (1989).
[72] P. Steiner, S. Hufner, A. Jungmann, V. Kinsinger and I. Sander, High T_c Superconductors: Electronic Structure, (Eds. A. Bianconi and A. Marcelli), Pergamon Press, Oxford, (1989).
[73] A. Bianconi, A.M. Flank, A. Fontaine, P. Lagarde, A. Marcelli, M. Verdaguer, J. Jegoudez, A. Revcolevschi and G. Demazeau, Physica C 153-155 (1988) 117.
[74] A. Bianconi, M. De Santis, A. Di Cicco, A.M. Flank, A. Fontaine, P. Lagarde, H. Katayama-Yoshida, A. Kotani and A. Marcelli, Phys. Rev. B 38, (1988) 7196.
[75] A. Bianconi, P. Castrucci, A. Fabrizi,A.M. Flank, P. Lagarde, S. Della Longa, A. Marcelli, Y. Endoh, H. Katayama-Yoshida and Z.X. Zhao, High T_c Superconductors: Electronic Structure, (Eds. A. Bianconi and A. Marcelli), Pergamon Press, Oxford, (1989).
[76] G. Kaindl, D.D. Sarma, O. Strebel, C.T. Simmons, U. Neukirch, R. Hoppe and H.P. Muller, Physica C 153-155, (1988) 139.
[77] J. Fink, N. Nucker, H. Rombeg and S. Nakai, High T_c Superconductors: Electronic Structure, (Eds. A. Bianconi and A. Marcelli), Pergamon Press, Oxford, (1989).
[78] A. Bianconi, M. De Santis, A.M. Flank, A. Fontaine, P. Lagarde, A. Marcelli, H. Katayama-Yoshida and A. Kotani, Physica C 153-155, (1988) 1760.

[79] C. Taliani, R. Zamboni, G. Ruani, A.J. Pal, F.C. Matacotta, Z. Vardeny and X. Wea, High T_c Superconductors: Electronic Structure, (Eds. A. Bianconi and A. Marcelli), Pergamon Press, Oxford, (1989).
[80] M. Bacci, Chemical Physisc 104, (1986) 191.
[81] M. Bacci, Japanese Journal of Applied Physics 27, (1988) L1699.
[82] H.P. Geserich, G. Scheiber, J. Geerk, H.C. Li, G. Linker, W. Assmus and W. Weber, Europhysics Letters 6, (1988) 277.
[83] A. Bianconi, P. Castrucci, M. De Santis, A. Di Cicco, A. Fabrizi, A.M. Flank, P. Lagarde, A. Marcelli, C. Politis, H. Katayama-Yoshida, A. Kotani and Z.X. Zhao, Modern Physics Letters B 2, (1988) 1313.
[84] C. Castellani, C. Di Castro and M. Grilli, Physica C 153-155, (1988) 1659.
[85] C. Castellani, C. Di Castro and M. Grilli, Proceedings of the Conference Towards the theoretical understanding of high T_c superconductors - Trieste, (Eds. S.Lundqvist, E.Tosatti, M.P. Tosi and Yu Lu), Int. Journal of Modern Physics 1, (1988) 659.
[86] H. Kamimura, Proceedings of the Conference Towards the theoretical understanding of high T_c superconductors - Trieste, (Eds. S.Lundqvist, E.Tosatti, M.P. Tosi and Yu Lu), Int. Journal of Modern Physics 1, (1988) 699.
[87] W. Weber, Z. Phys. B - Condensed Matter 70, (1988) 323.
[88] W. Weber, Advances in Solid State Physics 28, (1988) 141.
[89] M. Jarrell, H.R. Krishnamurthy and D.L. Cox, Phys. Rev. B 38, (1988) 4584.
[90] A.L. Shelankov, X. Zotos and W. Weber, Physica C 153-155, (1988) 1307.
[91] T. Nishino, M. Kikuchi and J. Kanamori, Solid State Commun. 68, (1988) 455.
[92] J. Askenazi and C.G. Kuper, Physica C 153-155, (1988) 1315.
[93] J. Askenazi and C.G. Kuper, High T_c Superconductors: Electronic Structure, (Eds. A. Bianconi and A. Marcelli), Pergamon Press, Oxford, (1989) and references therein.
[94] S. Kurihara, Physica C 153-155, (1988) 1247.
[95] A. Fujimori, High T_c Superconductors: Electronic Structure, (Eds. A. Bianconi and A. Marcelli), Pergamon Press, Oxford, (1989).